Spintronic Sensors Based on Magnetic Tunnel Junctions for Wireless Eye Movement Gesture Control

Asfand Tanwear, Xiangpeng Liang, Yuchi Liu, *Student Member, IEEE*, Aleksandra Vuckovic, Rami Ghannam, *Senior Member, IEEE*, Tim Böhnert, Elvira Paz, Paulo P. Freitas, Ricardo Ferreira, and Hadi Heidari, *Senior Member, IEEE*

***Abstract*—The tracking of eye gesture movements using wearable technologies can undoubtedly improve quality of life for people with mobility and physical impairments by using spintronic sensors based on the tunnel magnetoresistance (TMR) effect in a human–machine interface. Our design involves integrating three TMR sensors on an eyeglass frame for detecting relative movement between the sensor and tiny magnets embedded in an in-house fabricated contact lens. Using TMR sensors with the sensitivity of 11 mV/V/Oe and ten <1 mm^3 embedded magnets within a lens, an eye gesture system was implemented with a sampling frequency of up to 28 Hz. Three discrete eye movements were successfully classified when a participant looked up, right or left using a threshold-based classifier. Moreover, our proof-of-concept real-time interaction system was tested on 13 participants, who played a simplified Tetris game using their eye movements. Our results show that all participants were successful in completing the game with an average accuracy of 90.8%.**

***Index Terms*—Eye movement control, human-machine interaction, spintronics, tunnelling magnetoresistance sensor.**

I. Introduction

THE studies of eye movements and gestures is of interest to clinical ophthalmologists and psycholinguists [1], [2]. Eye gesture recording enables researchers to study potential eye disorders while performing various dynamic tasks. In 1981, Bolt was among the first to demonstrate the use of eye movements in human-computer interaction [3], [4]. Eye movement tracking is considered a robust method for gesture control, since these movements do not deteriorate with age, as those of other body parts do [1], [5]. Consequently, wearable devices that rely on tracking and classifying eye gestures have increasing utility in communication and control for people with high levels of physical or communicative disabilities. For example, individuals with physical disabilities can use wearable devices to control their wheelchairs using eye gestures [6], [7]. Eye-computer-based interaction provides an effective alternative to joystick-based control of mobility scooters for people who cannot functionally use their upper limbs [8]–[10]. It represents a novel approach for human-machine interaction and assisted living [11]–[15]. In addition, eye tracking provides an additional hands-free level of control for non-disabled people during fast, cognitively demanding tasks such as driving or flying. Furthermore, clinical ophthalmology research aims to resolve eye disorders by finding links between eye movement and other activities such as sports, mental attention and sleep [16]–[18].

Traditionally, eye movement detectors have used near-infrared (NIR) light transmitters and cameras to produce bright-dark contrast for pupil detection [19], [20]. Although not all eye types and NIR wavelengths produce the desired effect from corneal reflection, the relative distance between pupil and corneal reflection can provide useful gesture information [21]. However, mobile NIR devices typically cost around $10,000 and their desktop counterparts cost $5,000 [16]. Such high costs impede further market penetration by eye interface-based systems. Although alternative methods using web cameras are considerably cheaper, their dependence on lighting conditions makes such systems prone to errors induced by light interference [8], [22]. Likewise, infrared cameras are prone to infrared light interference [23] and both image-based and infrared-based cameras are susceptible to problems due to the top eyelid obstructing the iris, and head movement causing location error [16]. Additionally, desktop-based web cameras or NIR-based systems require participants to remain stationary, at a distance of around 70 cm from the camera or screen [8], [23]. This limits the applicability of eye gesture detectors.

Other approaches involving cameras include blink detectors, where blinking either with the right, left or both eyes trigger

Manuscript received June 14, 2020; revised July 31, 2020 and September 16, 2020; accepted September 21, 2020. Date of publication September 29, 2020; date of current version December 30, 2020. This work was partially supported by the UK EPSRC under Grant EP/R511705/1, and Grant PEER1819/03 from the Scottish Research Partnership in Engineering (SRPe). AT acknowledges support by the UK EPSRC DTP under Grant 2126385 *(Asfand Tanwear and Xiangpeng Liang contributed equally to this work). (Corresponding author: Hadi Heidari.)*

Asfand Tanwear, Xiangpeng Liang, Yuchi Liu, Aleksandra Vuckovic, Rami Ghannam, and Hadi Heidari are with the James Watt School of Engineering, University of Glasgow, G128QQ Glasgow, U.K. (e-mail: a.tanwear.1@research.gla.ac.uk; x.liang.1@research.gla.ac.uk; y.liu.7@research.gla.ac.uk; Aleksandra.Vuckovic@glasgow.ac.uk; Rami.Ghannam@glasgow.ac.uk; hadi.heidari@glasgow.ac.uk).

Tim Böhnert, Elvira Paz, Paulo P. Freitas, and Ricardo Ferreira are with the International Iberian Nanotechnology Laboratory (INL), 4715-330 Braga, Portugal (e-mail: tim.bohnert@inl.int; elvira.paz@inl.int; paulo.freitas@inl.int; Ricardo.Ferreira@inl.int).

This article has supplementary downloadable material available at https://ieeexplore.ieee.org, provided by the authors.

Color versions of one or more of the figures in this article are available online at https://ieeexplore.ieee.org.

Digital Object Identifier 10.1109/TBCAS.2020.3027242

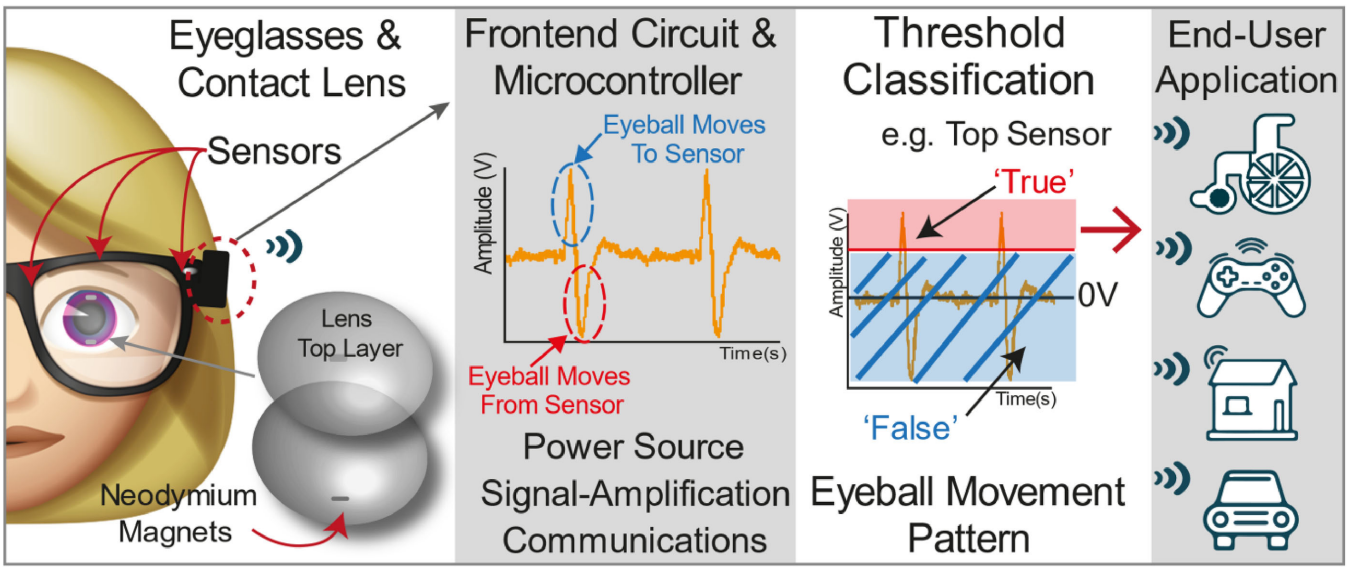

Fig. 1. Developed contact lens with embedded magnets that are detected and monitored by the TMR sensors within the glasses frame. Gestures are detected when the user gestures either up, left, or right, towards the sensors on the edge of the frame. Gestures are classified when amplitude thresholds are met. This system allows user to control systems such as wheelchairs.

different commands. However, it is difficult to differentiate between casual involuntary blinking and intentional user-evoked blinking [24]. The former is particularly pronounced under fatigue, causing the person to blink more often [25], requiring focus and stamina, which are often compromised in patient populations, to prevent unintentional blinking [26]. Therefore, the activation command/procedure should be used to allow the user to activate or deactivate the cameras on-demand for either blink or eye gesture detection.

Electrooculography, electromyography and electroencephalography can be used for human-computer interaction [27], [28]. However, these techniques are either too expensive, or too uncomfortable for the wearer, particularly if requiring multiple electrodes to be attached to the face [16], [29].

In contrast to the above, a novel eye gesture detection system is proposed that is highly reliable yet wearable and unobtrusive to the user. The sensing system employs thin-film spintronic sensors based on the tunnel magnetoresistance (TMR) effect integrated into a wearable eyeglasses platform. We demonstrate this proof-of-concept (Fig. 1) using ten <1 mm^3 cylinder-shaped magnets embedded within a contact lens and tested on an animatronic artificial eye model. This lens produces a changing magnetic field around a custom-built frame in the form of eyeglasses. By using sensitive magnetic sensors located on the frame, these magnetic differences can be captured and used to translate eye movements into a set of commands. This eyeglasses technology concept will be 3D-printed, as individuals have different head/face shape and will ensure almost similar performance compared to the experiment within this study. This customisation is essential, as when the magnetic sensor to contact lens separation is increased, the likelihood of magnetic field detection will decrease.

TMR sensors have greater sensitivity than other thin-film magnetic sensors, such as anisotropic magnetoresistance (AMR) sensors, giant magnetoresistance (GMR) or Hall-effect sensors [30]. It is noteworthy that TMR sensors are generally between 10 and 100 times more sensitive [31]. Furthermore, their lower bias current and comparably lower sensor size make TMR sensors a viable choice for wearable sensing technologies [32].

Another advantage of using a TMR sensor for eye gesture detection is its inability to detect ultra-low fields from skeletal muscles [33]. This is the case because the sensor is not attached to the face to detect weak magnetic fields, unlike in electrooculography, where artefacts generated by eyelid movement, blinking and facial muscle activation have been shown to interfere with eye movement recordings [34].

TMR sensors are based on a promising technology in spintronic research, in which conventional electronics make use of charge carrier mobility for either information or power transfer [35], [36]. Spintronics uses an extra degree of freedom from electrons, commonly referred to as 'spin', where electrons intrinsically spin upon their axis in either a clockwise (spin-up) or anti-clockwise (spin down) direction [37].

During stable operation, the TMR sensor's output signal is generated by altering its resistance. This is achieved by enabling or restricting the electron's quantum tunnelling probability. Specifically, resistance will vary depending on the free layer's orientation with respect to the pinned layer [38]. If both are parallel, higher tunnelling probability is achieved, which translates to lower resistance. Similarly, an anti-parallel alignment will result in a higher resistance, since more electron spin is reflected prior to the tunnel barrier due to spin-dependent scattering [35], [37].

In this paper, novel approaches are explored for eye gesture classification. In the next section, we provide a description of our methods for sensor development, followed by a discussion on the contact lens platform, TMR sensor integration, circuit design, the animatronic eye model, as well as the signal processing and decision-making process. In section 3, the experimental setup

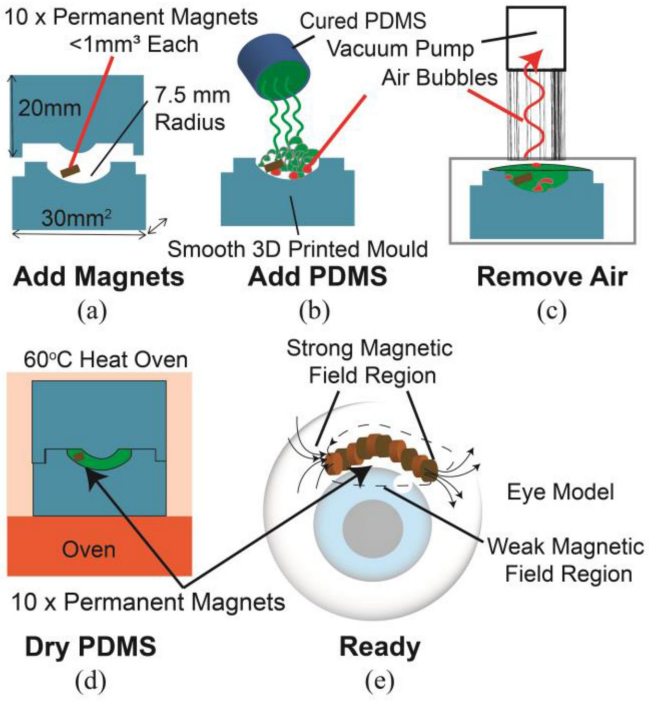

Fig. 2. (a) Permanent magnets are added to the 3D-printed, surface smoothed mould; (b) PDMS liquid is added to the magnets; (c) air bubbles are removed by vacuum pump to ensure a wearable lens; (d) the mould is added to the oven to solidify the liquid PDMS; (e) when the PDMS has solidified, the lens is peeled from mould and ready for use.

is described. In section 4, results, and experimental verification of 13 participants are presented. Finally, concluding remarks in section 5 are provided.

II. Materials and Methods

A. Contact Lens Fabrication

For the eye-gesture based system shown in Fig. 1, the magnets-embedded soft contact lens was fabricated. The N42 Neodymium (F305-100, first4magnets) permanent magnets were added into a 3D printed mould with polydimethylsiloxane (PDMS). The magnets were positioned off-centre to ensure the centre is as thin as possible for clear vision through the pupil and fit the mould. Each of the ten magnets was cylinder-shaped with 1 mm diameter and thickness providing less than 1 mm^3 in volume each. As shown in Fig. 2, the PDMS material and curing agent were mixed and then slowly poured into the mould with the magnets to ensure equal distribution. The fabricated material was placed in a vacuum chamber for one hour to prevent air bubbles from forming around the magnets and within the PDMS material. To accelerate the drying process, the mould was placed in an oven at 60 °C for 24 hours.

The 3D-printed mould was made from PolySmooth^{TM} printing filament, and the rough surface was smoothed with alcohol vapour gas using a PolySher^{TM} machine. An exposure time of 15 mins provided the best results when using 100% infill from the PolySmooth^{TM} filament. The smoothness of the mould increases with an increased exposure time, but over-exposure may cause its dimensions to alter, since the 3D-printed mould was based on the eye's real curvature, over-exposure will degrade the contact lens' wearability [39]. Use of 3D moulds has been reported in the literature, and the rough surfaces resulting from 3D-printing found to be problematic [40], causing user discomfort due to friction from the contact lens surface [41]. Therefore, alcohol vapour was used to smooth the 3D mould, while the use of PDMS ensured the lens was both soft and biocompatible to provide user comfort [42]–[44].

B. Tunnelling Magnetoresistive Sensor

The TMR sensors were fabricated with a nominal resistance of 1.75 kΩ, obtaining a measured sensitivity of 11 mV/V/Oe (Oersted) at 1 Volt(V) bias [45]. Increasing the bias voltage lowers the magnetoresistance (MR) ratio, which adversely affects the sensitivity of the device [35], [46], [47]. With zero bias voltage, the sensor's MR ratio was found to be 133%, and was expected to slightly decrease with increased voltage. Therefore, to maintain both high sensitivity and a large amplitude for the TMR sensor, the circuit was 5 V bias limited.

The selected TMR sensor that can detect the magnetic field of 115 pT at 196 Hz [45] was developed with a double pinned stack linearised in bulk with the three annealing strategy, increasing the sensor's linear response by post-deposition annealing at different temperatures [48]. Where the first annealing step was at 330 C with a bias field of 1 T applied for 2 hours. The second step at 270 C, applying 1 T perpendicular to the first annealing field direction for 2 hours. And the third step at 150 C with a field of 0.02 T parallel to the first annealing direction for 1 hour. Further details are available from Paz *et al.* [48]. Hence, with a linear response from the sensor allows the signal from each gesture to be reliably compared as an output voltage when the field strength from the contact lens is unknown [49].

Each of the three TMR sensor chips comprised 1102 TMR circular pillars of 100 μm diameter, connected in series to increase the area for magnetic sensing, since signal-to-noise ratio (SNR) is inversely proportional to the sensing area. Increasing the sensing area improved the likelihood of detecting magnetic fields originating from the contact lens, thereby improving the available signal output. Sensor placement is important since fields perpendicular to the top layer are less likely to be detected. This is because the sensor detects in-plane fields found within the free layer. As shown in Fig. 3, the magnetisation vector of the free layer with respect to the pinned layer determines the measurable resistance [50]. Therefore, if the TMR sensors were placed on eyeglasses, they would be located on the frames to detect in-plane fields. The sensors were placed flat on the 3D-printed frame at three locations, representing the top, left and right side of the spectacle frames, an area surrounding the glass lenses to prevent vision obstruction. Measured from centre of each sensor, the right and left sensors are 5.7 cm apart (horizontal), whilst the top (up) sensor is in between i.e. 2.85 cm (horizontal) and has a vertical separation height of 2.2 cm from the right/left sensors, this is to account for smaller vertical eye movements and designs seen from eyeglasses such as the Ray-Ban Wayfarers (RB2140) [16]. The vertical height of the right/left sensors is 4.7 cm from

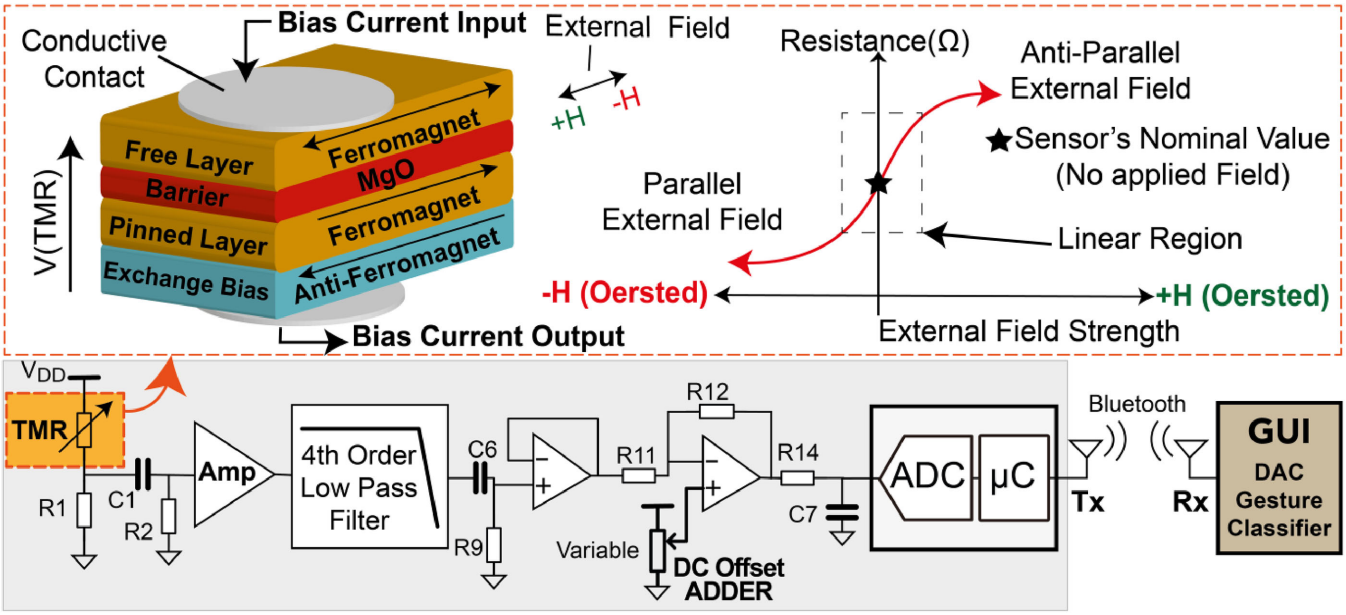

Fig. 3. Fabricated TMR sensor that varies resistance depending on the direction of the external field (magnetic eye lens) with respect to the pinned layer. The circuit is connected to a computer wirelessly via Bluetooth and classifies the signal from the wearable unit PCB into eye gesture commands.

the ground. The eye model was placed in between the right/left sensor and will be 2 cm away from the frame.

To produce a signal output, the TMR sensor needs to be current-biased and in series with a nominal resistance-matching resistor. For this study, a single TMR sensor alongside a 1.75 kΩ resistor was used for each of the three gesture directions. This method is susceptible to thermal drift, with a DC offset output equivalent to half the voltage bias (2.5 V), and must be filtered to enable amplification without saturation [51]. To reduce thermal drift and provide greater output with a measured sensitivity at 190 mV/V/Oe, a full bridge sensor configuration should be used. However, in this study, that was not feasible due to limited space. Each of the three sensors in this study consisted of a single TMR sensor.

The system was designed to obtain, top, right and left binary movements. It was previously mentioned in the literature that eyeball movement in the y-direction (vertical) is small and harder to differentiate, relative to when a subject is initially looking straight ahead [16]. Consequently, two directions along the x-axis (left and right) and only one vertical direction (up) were discriminated, with respect to looking straight i.e. centred position of a subject's eyeball gaze.

C. Circuit Design

To improve signal quality, a robust front-end circuit was required to remove external noise and improve the SNR, as shown in Fig. 3.

1) Bias Circuit: The readout from each TMR sensor was obtained via a front-end circuit and was powered by a single shared ± 5 V power supply unit. Each TMR sensor was matched with its nominal equivalent value resistor to create a voltage divider circuit, such that the front-end circuit measured the voltage change at the nominal resistor. Since the magnetic field was a few micro-Tesla at a 2 cm distance between the lens and TMR sensor, the magnetic field fell within the linear region of the TMR sensor (see the graph of resistance vs external field strength in Fig. 3). The output voltage was small and required amplification. Additionally, the sensor and the resistor were nominally matched, a large 2.5V DC offset was present.

2) High-Pass Filter: To remove the large DC offset before amplification, a first-order high-pass filter at C1 and R2 with a cut-off frequency of 0.5 Hz was used. Also, at C6 and R9 having the same cut-off frequency was based on data from the literature suggesting the minimum frequency for eye movements caused by eye fixation to be greater than 0.15 Hz [52]. Baseline drift filters are typically set to remove frequencies below 0.8 Hz coming from various sources, such as slow varying environmental magnetic fields [53] or the thermal drift of the TMR sensor itself [54] that could interfere with the circuit [55]–[57]. This is advantageous for noise reduction since frequencies $<$0.8 Hz are somewhat attenuated when the 3-dB point is set at 0.5 Hz, without effecting the eye gesture signals found at frequencies $>$0.8 Hz.

3) Amplification: During initial testing, the signal amplitude from a moving contact lens was found to be smaller than 50 mV and thus required further amplification to reduce the influence of electronic noise from filters and the input noise of the microcontroller (Bluno Beetle); better SNR also improves classification accuracy. An operational amplifier (Texas Instrument OPA4227) with very low noise input 3 nV/$\sqrt{}$Hz and a closed loop gain of 400 was used. This ensured an output signal in the volts range, which was sufficiently high for an amplitude threshold-type classifier.

4) Low Pass Filter: The typical sampling frequency range of mobile eye-tracking systems is between 25–60 Hz [17].

A two-stage 4th order Butterworth active low pass filter was therefore designed with a cut-off frequency of 28 Hz and a sampling frequency of 60 Hz. High-frequency micro eye movements (micro-saccades), which can reach up to 1000 Hz [1], were thus attenuated to avoid interfering with the eye gesture recordings. In addition, the filter attenuated 50 Hz powerline and other high-frequency magnetic field noise found within the environment [53].

5) Analogue-to-Digital Conversion (ADC), Protection and Transmission: The 'DFROBOT Bluno Beetle' was used, as it is capable of both Bluetooth transmission and multichannel ADC. The built-in ATmega328p chip can convert analogue-to-digital signals at 10-bits (0 to 1023 steps) with a voltage range of 0–5 V. This voltage was within the allowed supply voltage range (-0.6–5.6 V) for the ADC pins. Additionally, using a difference amplifier configuration, a DC offset of 2.5 V was added to the final output. This allowed the signal to swing to the midpoint of the voltage supply, such that the output signal could reflect field polarity changes.

The signal was then transferred via Bluetooth to a computer for data processing and classification using a voltage threshold classifier. The signal amplitude increased, creating a positive peak, during a gesture that moved the eyeball towards the senor, and produced a negative peak when gesturing away from the sensor. The time-delay from the eye model's gesture movement to the PC classifier, via the analogue front-end of the TMR sensor was determined to be up to 1 second. This delay was a result of the circuit delay, mainly from filters, as well as communication delay between the PC and microcontroller circuit.

D. Animatronic Eye Model

Before performing an on-body human test, our proof-of-concept system was non-invasively validated using a custom-built gaze following system (GFS), as shown in the supplementary (2). Stringent test is required for a contact lens, as discomfort and risk of eye infection must be mitigated before being considered for human use [58]. Alternative methods, as found in research on electrical contact lenses, were tested on animals either *in-vitro* [59] or *in-vivo* [60]. However, the animals cannot perform an on-demand eye command and interface with a computer. In the proposed system, a mimicking eye model was created to reduce lag-time by safely testing the feasibility of the proposed magnetic sensor and front-end circuit before a validated wearable lens design.

During the experiment, the user's gaze direction was mapped onto an artificial animatronic eye model wearing a magnetic contact lens. The magnetic contact lens was attached to the eye model and used two servo motors to control its movements. The animatronic mechanism moved the eyeball by mimicking eye movement from a human volunteer via an optical camera. In the GFS, the relative coordinates between the centre of the eye and pupil were extracted from the video data using image processing and gaze tracking algorithms. By controlling the servo motors, the eye model was able to follow the user's eye movement with less than 100 milliseconds (ms) delay. Volunteers were requested to move their eyeball to discrete locations by looking up, left and right.

A commercial eye (OEMI-7) matching the dimensions of a typical human eyeball was used. A single servo-controlled movement in the x-axis (horizontal), and another in the y-axis (vertical). The eyeball was approximately 24 mm in diameter, with a pupil diameter of around 7 mm. The model was surrounded by an outer protection holder, expanding the diameter to 35 mm, and adding both size and weight to the animatronic eye model.

To overcome this challenge, the animatronic mechanism was 3D-printed, and the eye model was attached to the 3D structure via a nickel-coated iron universal joint. The joint was 7 cm from the sensor and 5 cm from the lens. When initially tested within a shielded environment, the metallic joint was found not to disrupt the magnetic field sensed at the TMR sensor and when compared to a 3D-printed plastic joint movement, it was found to be more fluid. The joint allowed the eyeball to be pulled into different positions by the 9-gram servo motor using rigid metallic wires with low friction. Due to the design of the eye model such as the OEMI-7, the centre of the eyeball could not be accessed therefore, the centre of eyeball rotation (CER) had to be outside the eyeball and the eye's centre-of-mass point was no longer at a fixed position. The universal joint was placed behind the model and was the new centre of rotation. The eye model moved unnaturally, as for each degree of movement detected by the webcam, the eye model moved more. To mitigate this issue as much as possible, calibration of the servo motors was required when mapping each gesture position. The control of the two servo motors was programmed with a high-speed microcontroller. The GFS software application converted eye movements from the optical camera into a pulse-width-modulation signal for controlling servo motors. The GFS software coded with LabVIEW ^{TM} was able to transmit eye positions via a USB 2.0 cable, this allowed interface between the PC and the microcontroller, and process the signal transmitted from the Bluetooth enabled front-end circuit. The restricted motor movements were proportional to the range of movement of a human eyeball, allowing rotation in the horizontal direction for 180 degrees from corner to corner of the eyelid, and for 130 degrees in the vertical direction, to replicate the limitations of a real eye [20]. This may still result in slightly larger than lifelike movements [61], and for a real-life scenario would mean the source magnetic field will be reduced per gesture. To mitigate such problems in real-life, solutions can be employed such as improved sensor's sensitivity (or detectivity) levels, custom eyewear design (to reduce sensor and lens separation) or signal amplification. However, signal amplification is depended on the system's signal-to-noise ratio (SNR) and hence system's SNR improvements techniques would also be employed.

E. Signal Post-Processing and Decision Making

In the current system, a signal corresponding to eye movement is post-processed before being sent to a decision-making algorithm to reconstruct the eye movement. There are four steps in the software's built-in signal processing [62].

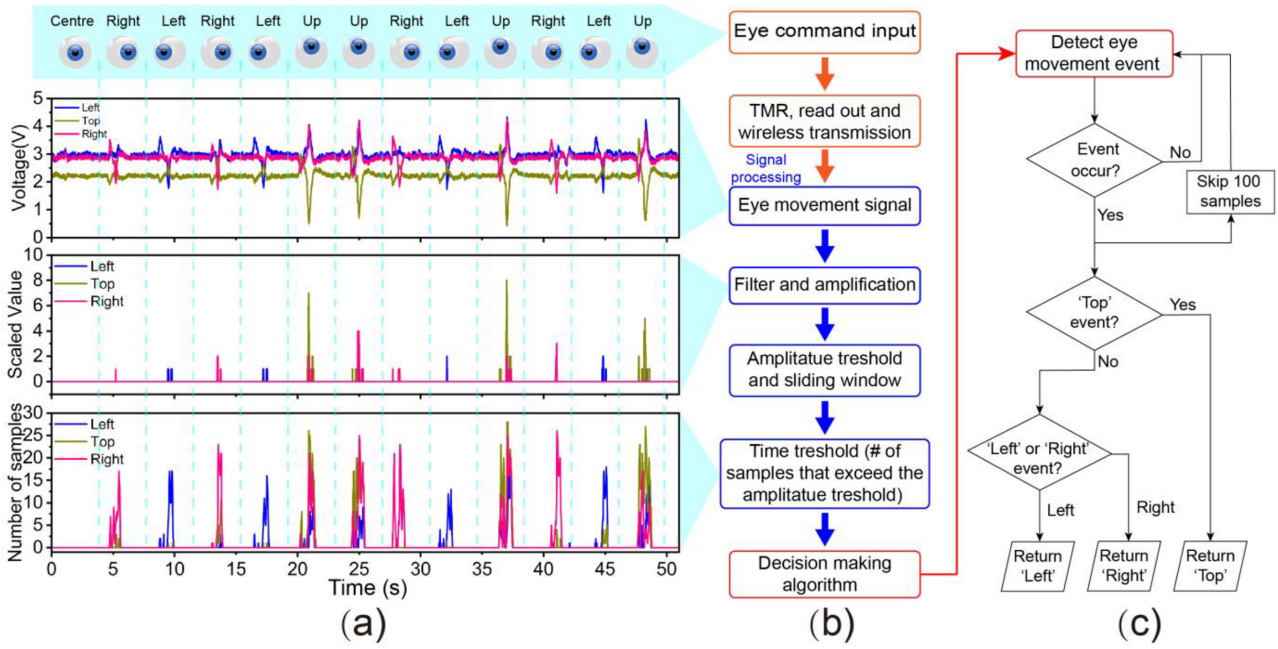

Fig. 4. (a) Shows the voltage amplitude threshold in operation, whereby up, left and right gestures are classified using scaled value to improve the distinction between each gesture; (b) depicts the block diagram of the entire system's sequence of operation both in hardware (black) and software (blue); (c) presents the flow chart of the decision-making algorithm.

1) Eye Movement Signal: Fig. 4(a), shows an example of the signal received via wireless readout circuit in response to different eye movement. Flow charts depicting signal post-processing and decision-making are presented in Fig. 4(b) and Fig. 4(c), respectively. Generally, a higher peak-to-peak signal occurred, as the eye and contact lens got closer to the sensor. For example, the left sensor returned a higher value when the eye looked to the left, while the signals from the sensor located to the right and up remained low. The opposite occurred when the eye looked to the right. When the eye looked upwards all three sensors produced high amplitude signals, but that was the only condition in which the "upwards" sensor produced a high amplitude signal. In this study, movement of the left eye was tracked, although the right eye can be used, as well.

2) Filtering and Amplification: To remove DC drift, a 2nd order Butterworth high-pass filter with a cut-off frequency of 0.5 Hz was applied. To amplify the difference between each eye movement and noise peaks, the signal was taken to the fourth power.

$$s_m(n) = f(u_m(n), c)^4 \tag{1}$$

where the $u_m(n)$ and $s_m(n)$ represents the input and output of m^{th} sensor respectively (in the current design m = {1, 2, 3}), f(x) is the filter function, c is the coefficient of the DC removal filter. The corresponding signal is illustrated in Fig. 4(a). After filtering and amplifying the signal, the response of the movement was enhanced, and the artefact was attenuated. This operation facilitated signal thresholding in the next step.

3) Amplitude and Time Thresholding: Afterwards, amplitude thresholds were determined heuristically and set independently for signals coming from each of the three sensors independently. To separate the real signal from fluctuating noise and other unexpected movements, the number of samples that exceeded the amplitude thresholds was calculated in a sliding window of 100 samples (approximately 1 second). If we define a thresholding function as:

$$h_k(x) = \begin{cases} 1 \text{ for } x \geq t_k \\ 0 \text{ otherwise} \end{cases} \tag{2}$$

The operation of this step can be described as:

$$y_m(n) = h_2\left(\sum_{i=n-L}^{n} h_1(s_m(i))\right) \tag{3}$$

where L denotes the length of the sliding window (L = 100), the $y_m(n)$ is the event occurrence flag of the m^{th} sensor that will be sent to the next step. There were two threshold values, t_1 and t_2, in the h_1 (amplitude threshold) and h_2 (time threshold), respectively. Both values were empirical numbers obtained during system development. Where time threshold ensures an event was captured, only when the spiking signal existed longer than a certain period. The amplitude threshold captured the spike generated by a changing magnetic field while, the time threshold evaluated the spike width for distinguishing eye movement signal peaks and other fluctuating noise, such as head movement. Afterwards, the threshold triggered an eye movement event for the next step, decision-making.

4) Decision Making: As explained above, when participants looked upwards, an increase in signal amplitude was noticeable with all three sensors, while for looking left and right, only the corresponding sensors closest to the iris were responsive. As shown in Fig. 4(c), the algorithm first investigated the signal from the top sensor. If the amplitude was above the threshold

for a predefined period, this event was labelled as 'up', irrespective of the condition of signals from the other two sensors. If the signal from the top sensor remained under the threshold, signals from the left and right sensors were analysed to detect the direction of eyeball movement. After receiving an event, the system stopped detecting upcoming events for another 100 samples to avoid activation by unintentional movements such as e.g. a saccade, when a person typically briefly looks from left to right or vice versa.

III. Experimental Setup

A. Participants and Experimental Procedures

Thirteen participants took part in the study. There were 11 males and 2 females. Their mean age was 27.7 years, with $\pm$ std. 4.5. The minimum age of the participants was 24 years, and the maximum was 38 years old. All participants signed a consent form prior to taking part in the study, which was approved by the University's ethical committee. To test the eye gesture system, participants were invited to play a custom-built eye gesture-based game, inspired by Tetris [63]. Participants sat approximately 70 cm from a 15- inch computer screen. Prior to taking part in the experiments, participants completed a brief 5-minute familiarisation session in which they learned how to play the game and tested each gesture at least once. Also, each user would need to have little or no head movement to reduce gaze-tracking error for the eye model via the web camera [20], wherein some users may feel it to be unnatural or tiresome and need time for system familiarisation.

The objective of the game was to complete a row of four blocks. Each block was moved down by the participant looking up. The block moved to the right when the participant looked right, and to the left when they looked left. Once a block reached the bottom, the participant needed to provide an 'up' command to lock the box and bring down a new block from the top of the game. When the final block was placed, the participant had to look up one more time to complete the game. The purpose of the game was to allow participants to determine the movements on their own, but the objective of the game was the same for all participants. For that reason, the total number of movements, and the number of movements in left, right and up directions varied among participants. The Tetris game can be completed with 24 correct commands using four blocks. Whereby based on early feedback, the four blocks were sufficient to induce some fatigue, as users were continually sitting upright to face the camera and maintaining focus to determine their next move. Therefore, the experiment required limited commands, as using five or more blocks began to disengage users from the experiment with fatigue.

An advantage of using live participants is that the mimicking eye model may detect unique eye movements given that each user playing a game may produce incorrect commands and later would self-correct with the online interface system. The unwanted commands could either come from false classification or human decision error. Therefore, pre-recorded eye model movements are not used to test the proof-of-concept system, considering each eye gesture may be different when used for a real-life application and provided that each user will have the option to promptly self-correct after every incorrect command.

B. Test Setup

Fig. 5 shows the GFS software and hardware, along with the built-in wireless data acquisition and real-time signal processing systems. The participant's eyes were focused on the Tetris game window placed 1 cm below the top-centre corner in the 15-inch computer screen and 3 cm below the web camera. The game window was 3 cm^2. The participant had both eyes on the window and was free to move them within the window to assess the game.

To monitor the movement of the eye model, the experiment was recorded using a video camera. After each classification, an audible sound was generated. Three different sounds were used, identifying which sensor was activated. This allowed the experimenter to compare the sensor activated with the gesture made by the eye model, to determine the accuracy of the system.

IV. Results and Discussion

As shown in Fig. 6(a), the mean number of total moves to complete the game was 32 $\pm$ std. 7.1, and the total mean correct commands was 29 $\pm$ 5.8. Five participants with the fastest times ($<$1 min) for game completion finished the game in under 26.6 $\pm$ 0.9 moves, whereas the slower participants (1–4 mins) finished them in 35.9 $\pm$ 7.6 moves. The classification accuracy of each sensor from the 13 participants and the overall accuracy from the 'Tetris' game is illustrated in Fig. 6(b) The average mean accuracy was 90.8% $\pm$ 5.9%. The highest average individual accuracy was 96% and the lowest was 80%. For individual classification labels, the results show that, except with participant 10, the top sensor was classified with 100% accuracy, but it also had a high false positive rate. No user was able to achieve 100% accuracy concurrently for both the right and left sensors. For example, when an upward gesture was made, the left or right sensors incorrectly met the gesture threshold. This was partly caused by a camera error, which resulted in the eye model looking off-centre. Consequently, when an upward command appeared, the closest left or right sensors were incorrectly activated. A second potential cause was participants not looking perfectly to the centre; since the eye model was mimicking the gesture, this meant that the eyeball was also facing off-centre. This caused the closest sensor to trigger first before triggering the user's desired sensor. For example, since participant 2 was facing slightly left from the centre, an 'up' gesture was incorrectly triggered by the left sensor first. This resulted in the left sensor being 50% incorrectly classified for participant 2.

To further analyse the system can be achieved by measuring the information transfer rate (ITR) or also referred as bitrate, where the bitrate equation found in [64], [65], provides system performance of the human-computer interface in bits-per-minute. From the 13 participants, the mean group average bitrate (bits/min) is 26.7 $\pm$ std. 17. As the group's minimum, the bitrate of the slowest player to complete the trail (3 min 55 sec with 45 commands) was 6.5 bits/min whilst, for the fastest player (36 secs with 26 commands) the ITR was 56.8 bits/ min.

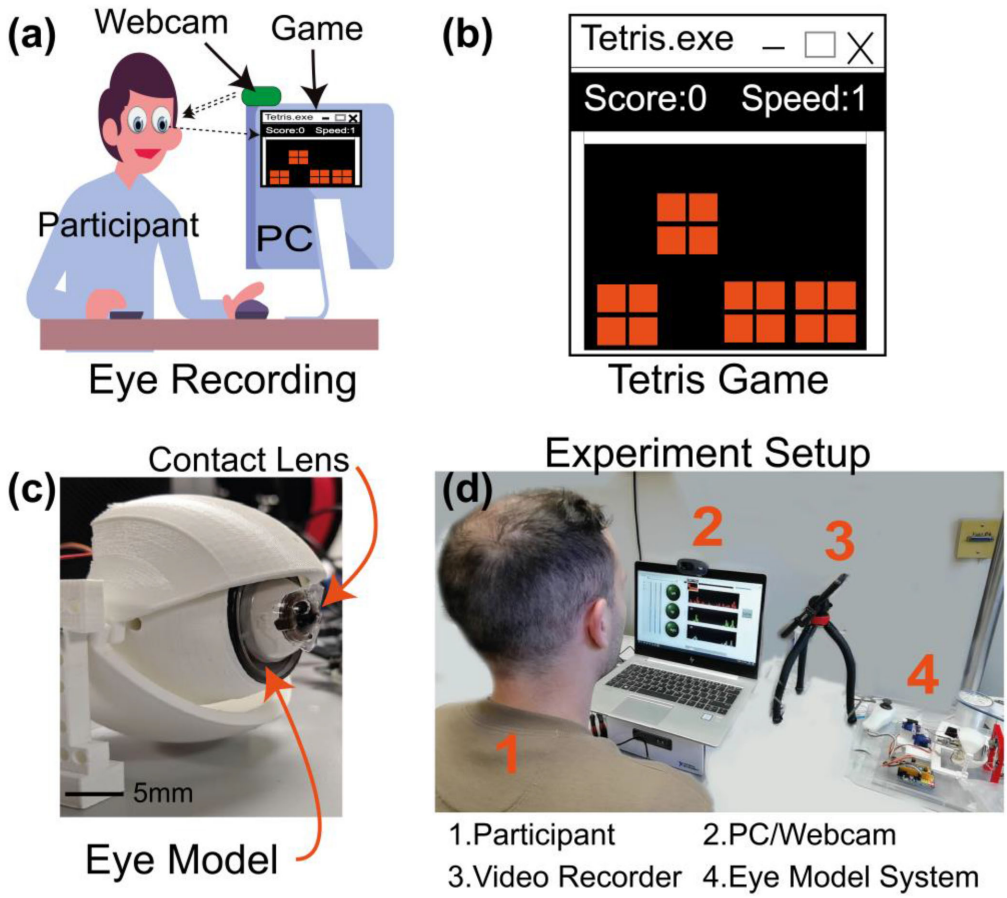

Fig. 5. (a) Illustration of a participant undertaking eye movement recording by playing the 'Tetris' based game via a webcam; (b) A screenshot of the 'Tetris' graphical interface that allows data recording; (c) The front of a GFS (gaze following system) with the magnetic embedded lens placed on the eye model; (d) the experimental setup of a participant undertaking eye movement recording by playing the 'Tetris' game, with the GFS mimicking eye movements.

The fastest four of the thirteen players have ITR greater than 40 bits/min. To account for the standard deviation of 17, the ITR number is shown to be affected by the nature of the Tetris game interface, where each trial was a self-paced open task and hence the duration of each trial and number of total commands varied between each player. To compare with other modalities, such as brain computer interfacing with electroencephalography, bit rate of 190 bits/min was recently achieved [66]. The bitrate is relatively higher and maybe attributed to the high number of target commands (48) whilst maintaining a similar accuracy of 90.3%, compared to our system accuracy at 90.8%. Additionally, each eye gesture movement speed from a user's voluntary action maybe slower than the speeds found when detecting electrical potentials from the brain and may account for the slower bitrates, as the trial time is prolonged further.

As a group mean average, the total commands used at each gesture direction were as follows: Left 9 ± 3.62, Right 4 ± 2.08, Up 16 ± 1.41. The commands per direction are not comparable as the Tetris game starting position was at the centre right-hand side and hence right command was the least used, where a maximum of eight right gesture commands was employed from two of the thirteen participants. This would also be the case, if the starting position were at the left-hand side and left command would be the least tested, hence a trade-off within a 4 block Tetris interface test. The up command was used more than the left/right command, as this command was needed to bring the block down from the top row and once placed in the last row, it would lock the current block and bring the next block. This repetition accounts for the larger gesture direction mean average.

A. *State-Of-The-Art Comparison*

Table I shows a comparison between our results with other eye gesture-based systems during the past 5 years. The average accuracy of the other systems was greater than 90% with ITR greater than 56 bits/min. Some of these methods deliver a very high accuracy at a high transfer rate, but are too large and immobile for realistic wearable applications [67]–[72]. The system demonstrated by Graybill *et al.* [73] involved developing smaller, more mobile, light insensitive and more inexpensive solutions. Their system was based on eye blinking, which may be difficult or tiring for some participants. However, our approach is different. In our design, with the omission of the bottom sensor, a user can easily rest between gestures by looking down or blinking, without affecting sensor detection. The user can have more control of the device, as a gesture is only registered

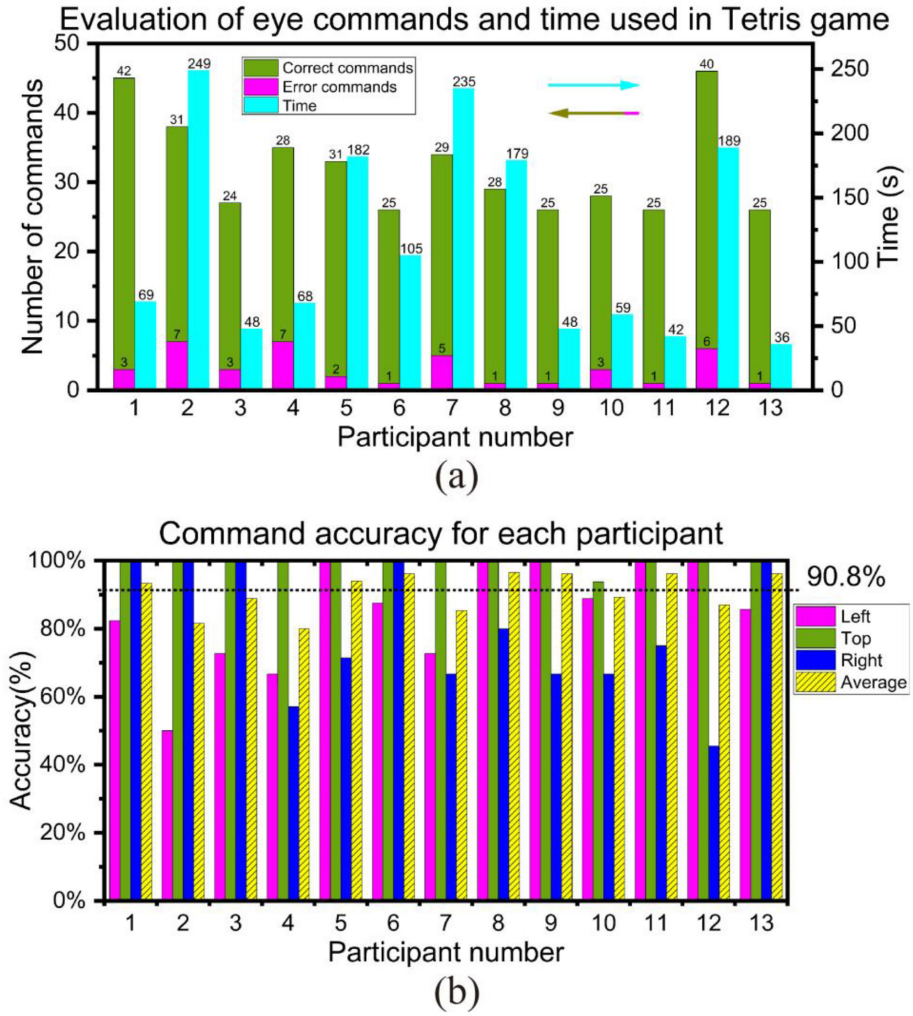

Fig. 6. (a) Results from 13 participants. The amount of correct commands is highlighted in green and the total in magenta. The blue bar shows the time each participant took to complete the same Tetris-based game; (b) the system's accuracy in classifying eye movement from the animatronic eye model, showing results for the left (magenta), top (green), and right (blue) sensors were classified. The top sensor achieved near perfect results. The average accuracy (yellow) indicates the highest average accuracy achieved by an individual was 96%.

when the eyeball moves from the centre and then towards one of the three sensors at a speed greater than 1 Hz. Therefore, slowly looking towards a sensor will not trigger it. This is an important distinction between eye gesture and blink gesture-based systems, since some participants may have conditions such as blepharospasm, which cause unwanted blinking or twitching. Whilst healthy participants can be affected by other unwanted eye lid movements such as a simple breeze of wind, which may cause the eyelid to shut. Compared with systems based on eye blinking, the advantage of our proposed solution is that resulting facial expression was less striking or noticeable by other people when compared to individuals making multiple (left or right) blinks with intent. Hence with eyeblink systems the user's face was found to animate more per gesture when interfacing with a device.

Our system has three inputs translating to three commands (up, left, right) that can be expanded to more commands depending on sequence and speed. For example, Graybill *et al.* [73] demonstrated that the three input eye gestures, which are the left (L) wink, right (R) wink or both (B) blinks, can be combined within a fixed time window to increase the total number of possible commands to eight, such as L, LL, LR, LB, R, RL, RR, and RB. Therefore, our system can also be expanded in a similar method using the 'up' gesture, instead of the 'both' blink gesture by Graybill *et al.* [73] Adding another TMR sensor in our system would not only increase the number of inputs, but it further increases the total combination of commands beyond eight.

B. Limitations

A limitation of the current solution, which is based on contact lenses is that it increases a setup time in comparison to solutions requiring glasses only, particularly if a disabled user needs to have the contact lens fitted by a caregiver. In addition, some users might be intolerant to wearing contact lenses as for the current version, the contact lens contains multiple <1 mm^3 magnets, the thickness, weight or size of these magnets may make it difficult to shut the eye or cause discomfort and obstruct vision. However,

TABLE I
PERFORMANCE SUMMARY AND COMPARISON TABLE OF THIS WORK WITH THE STATE-OF-THE-ART

Reference	Measured Target	Sensor Technology	Sensor package	Light Sensitive	Mobility	# User Input Actions	Cost	#Test Users	Mean Accuracy	ITR (bits/min)
Fathi *et al.* 2015 [67]	Visual blink detection	720P Web camera	PC based camera setup	Yes	Very Low	2 (slow & fast blink)	Camera (£20) excluding PC	30 (Offline)	97%	Not Available
Sato *et al.* 2017 [68]	Visual eye blink	Camera (1080p, 60FPS)	PC based camera setup	Yes	Very Low	3 (involuntary, slow & fast)	£60 excluding PC	10	95%	Not Available
You *et al.* 2017 [69]	Visual eye blink	Infrared Video	PC based Infrared camera setup	No	Very Low	3 (very slow, slow & fast)	£500 excluding PC	200 (offline)	91.6%	Not Available
Singh *et al.* 2018 [70]	Visual eye blink	720P Web camera	PC based camera setup	Yes	Very Low	3 (left, right & both eyes)	Camera (£20) excluding PC	10	89%	Not Available
Kowalczyk *et al.* 2018 [71]	Visual eye blink	Infrared Video	Two Infrared cameras mounted on glasses	No	Medium mobility	2 (left and right eye blinks)	Estimated £1000 excluding PC	30	99.68%	Not Available
Huang *et al.* 2018 [72]	Eye blink	Electro-oculography (EOG)	Electrode, processing box on Wheelchair	No	Medium, requires wheelchair	3 (left, right & both eyes)	EOG estimated £1250 excluding PC	8	96.7%	57.3
Graybill *et al.* 2019 [73]	Eye blink	Inductive	Wearable glasses & coil on eyelid	No	High	3 (left, right & both eyes)	Unknown ("low cost")	6	96.3%	56.1
This Work	Eyeball gesture	Magnetic sensor	TMR Sensor on eyewear frame & contact lens on eye model	No, (except it requires eye model camera)	Medium, (since requires eye model camera)	3 (left, right & up)	£37.50 Excluding PC	13	90.8%	26.7

in cases where the non-disabled user is exposed to fast changes of illumination conditions such as during driving or flying, the proposed system (Fig. 1) is clearly advantageous as compared to systems sensitive to light interference. In contrast, the system tested in this study needs to use a webcam and make gestures via an eye model and therefore light interference was found to be an issue. Where in this study, individuals with prescription glasses were not tested, as light interference may cause an issue when detecting and tracking the eye. Also, individuals with eye disease did not participate in this study, as they may have reduced control over their eye movements when testing for human-machine interface, even though the camera might be able to detect their eye movements.

Another limitation of this current system compared to a real eye is of their fluid eye movements, where extraocular muscles provide faster and more precise movements. The GFS resolution of movements is limited by the resolution of the PC computer/microcontroller to the servo motors and as such the eye model is not a replacement of a real eye. The eye model may still make faster (jerkier) motion than a real eye movement even though its rate of change falls below <28 Hz, even after being mapped during experiment design to ensure matched movements. Hence, to ensure a more realistic eye movement from the animatronic system, the centre of rotation needs to be centred within the eye model, then remeasured and remapped to ensure matched smooth movements. Therefore, the system would have to be upgraded and validated to ensure lifelike eye movements.

Additionally, the front-end system is insensitive to slow, subtle eyeball gesture movements and it was also found it works best when users focus their gaze. As previously explained, frequencies less than 1 Hz are attenuated by the high-pass filter. Therefore, participants must move their eyeball slightly faster than they might be accustomed to. For the sensor to detect a strong magnetic field, some participants needed to move towards the corners of their eye to move the lens closer to the magnetic sensors. Repeating this process can be fatiguing for participants. This might be problematic for patients with limited control of eyeball muscles, such as those suffering from amyotrophic lateral sclerosis that can have voluntary eye movements but may still feel fatigued overtime therefore, the system would require further development before being fully applicable to patients.

The results from the experiment were limited by the fact predetermined moves were not used, rather the task was open. As it allowed the user to self-determine strategies to get a quick time. This meant 'false positives' could not be measured, i.e. moves the user not intended but resulted in a favourable outcome, as the participant was making quick gestures making it difficult to track and compare eye gestures with the eye model. Furthermore, with limited commands, the game duration was at a maximum of 3 minutes 55 seconds, and with fatigue as a factor, analysis with longer experiment time was not included in this study.

One of the main limitations of the proposed proof-of-concept modality, even though this study took place in a non-shielded lab environment, is that the magnetic field noise may vary when outside the lab. Also, induced magnetic field such as from elevators, large head motions during recordings or introduction of other magnetic fields that are greater than a few micro-Tesla may interfere with the eye gesture recordings. A method to mitigate this noise is with the use of a trigger command by making a specific gesture towards a sensor with either eyeball. This will ensure gesture is not recorded continuously, for example, when an individual is running, and a large field is induced compared to when the user is at rest. Or when the user is performing a daily activity and does not require interfacing capabilities with the eye gesture system at that moment.

V. Conclusion

In this paper, we proposed a novel eye gesture detector using miniature TMR sensors with a sensitivity of 11 mV/V/Oe. We demonstrated that magnets embedded within the soft contact lens can create sufficiently strong magnetic fields to be detected by nearby sensors. Using a web camera to record participant eye movement, 13 participants successfully completed a 'Tetris' gesture-based game. A mean accuracy of 90.8% $\pm$ 5.9% was achieved using a proof-of-concept prototype with custom-built GFS. Our lens was placed on an animatronic eye model and the sensors were placed on a 3D-printed frame to substitute an eyeglass frame. The system successfully detected three eye gestures: Up, left, and right. These corresponded to the position of the TMR sensors on the frame. The purpose of the GFS is to validate the concept non-invasively. In conclusion, the results demonstrate the proposed method to be a strong candidate for future solutions in human-machine interfaces and assisted living. Further advancements of this work will involve (1) increasing the number of commands and accuracy by combining machine learning techniques and include more eye gesture pattern datasets such as circular movements, (2) optimising readout circuit by miniaturising the TMR sensors into bridge configuration for greater sensitivity and (3) developing a more efficient power unit with lower power consumption to ensure that the system is fully wearable.

Supplementary Information

Data availability: Data supporting the plots within this paper and other finding of this study are available from the corresponding authors upon reasonable request.

A demonstration of the system can be found via the following link: *Code and image availability:* Design of the eye model and software code can be found via the following GitHub link: **https://github.com/melabglasgow/Eye-gesture**. Also, found within the link is a closeup image of the GFS system.

References

[1] D. Wendt, T. Brand, and B. Kollmeier, "An eye-tracking paradigm for analysing the processing time of sentences with different linguistic complexities," *PLoS One*, vol. 9, no. 6, Jun. 2014, Art. no. e100186.

[2] K. Brogan, B. Dawar, D. Lockington, and K. Ramaesh, "Intraoperative head drift and eye movement: Two under addressed challenges during cataract surgery," *Eye*, vol. 32, no. 6, pp. 1111–1116, Jun. 2018.

[3] R. A. Bolt, "Gaze-orchestrated dynamic windows," *Assoc. Comput. Machinery*, Aug. 01, 1981. [Online]. Available: http://doi.org/10.1145/965161.806796., Accessed: Apr. 08, 2020

[4] R. A. Bolt, "Eyes at the Interface," in *Proc. Conf. Hum. Factors Comput. Syst.*, New York, NY, USA, 1982, pp. 360–362, doi: 10.1145/800049.801811.

[5] S. Dowiasch, S. Marx, W. Einhäuser, and F. Bremmer, "Effects of aging on eye movements in the real world," *Front. Hum. Neurosci.*, vol. 9, p. 46, 2015, doi: 10.3389/fnhum.2015.00046.

[6] A. M. Choudhari, P. Porwal, V. Jonnalagedda, and F. Mériaudeau, "An electrooculography based human machine interface for wheelchair control," *Biocybern. Biomed. Eng.*, vol. 39, no. 3, pp. 673–685, Jul. 2019.

[7] M. Subramanian, N. Songur, D. Adjei, P. Orlov, and A. A. Faisal, "A.Eye Drive: Gaze-based semi-autonomous wheelchair interface," in *Proc. 41st Ann. Int. Conf. IEEE Eng. Med. Biol. Soc. (EMBC)*, Berlin, Germany, Jul. 2019, pp. 5967–5970, doi: 10.1109/EMBC.2019.8856608.

[8] R. Naqvi, M. Arsalan, and K. Park, "Fuzzy system-based target selection for a NIR camera-based gaze tracker," *Sensors*, vol. 17, no. 4, Apr. 2017, Art. no. 862, doi: 10.3390/s17040862.

[9] C. Mauri, T. Granollers, J. Lores, and M. Garcia, "Computer vision interaction for people with severe movement restrictions," *Hum. Technol.*, vol. 2, no. 1, pp. 38–54, Apr. 2006, doi: 10.17011/ht/urn.2006158.

[10] R. O. Maimon-Mor, J. Fernandez-Quesada, G. A. Zito, C. Konnaris, S. Dziemian, and A. A. Faisal, "Towards free 3D end-point control for robotic-assisted human reaching using binocular eye tracking," in *Proc. Int. Conf. Rehabil. Robot. (ICORR)*, Jul. 2017, pp. 1049–1054, doi: 10.1109/ICORR.2017.8009388.

[11] S. Mathôt, J.-B. Melmi, L. van der Linden, and S. Van der Stigchel, "The mind-writing pupil: A human-computer interface based on decoding of covert attention through pupillometry," *PLoS One*, vol. 11, no. 2, pp. 1–5, Feb. 2016, doi: 10.1371/journal.pone.0148805.

[12] Y. Cha, J. Seo, J.-S. Kim, and J.-M. Park, "Human–computer interface glove using flexible piezoelectric sensors," *Smart Mater. Struct.*, vol. 26, no. 5, May 2017, Art. no. 057002, doi: 10.1088/1361-665X/aa6b64.

[13] A. Memo and P. Zanuttigh, "Head-mounted gesture controlled interface for human-computer interaction," *Multimedia Tools Appl.*, vol. 77, no. 1, pp. 27–53, Jan. 2018, doi: 10.1007/s11042-016-4223-3.

[14] S. Soltani and A. Mahnam, "A practical efficient human computer interface based on saccadic eye movements for people with disabilities," *Comput. Biol. Med.*, vol. 70, pp. 163–173, Mar. 2016, doi: 10.1016/j.compbiomed.2016.01.012.

[15] B. Bianchi, G. Bengolea Monzón, L. Ferrer, D. Fernández Slezak, D. E. Shalom, and J. E. Kamienkowski, "Human and computer estimations of predictability of words in written language," *Sci. Rep.*, vol. 10, no. 1, pp. 1–11, Mar. 2020, doi: 10.1038/s41598-020-61353-z.

[16] Y. Cheung and Q. Peng, "Eye gaze tracking with a web camera in a desktop environment," *IEEE Trans. Hum.-Mach. Syst.*, vol. 45, no. 4, pp. 419–430, Aug. 2015, doi: 10.1109/THMS.2015.2400442.

[17] R. Kredel, C. Vater, A. Klostermann, and E.-J. Hossner, "Eye-tracking technology and the dynamics of natural gaze behavior in sports: A systematic review of 40 years of research," *Front. Psychol.*, vol. 8, Oct. 2017, Art. no. 1845, doi: 10.3389/fpsyg.2017.01845.

[18] A. Brancaccio, D. Tabarelli, M. Bigica, and D. Baldauf, "Cortical source localisation of sleep-stage specific oscillatory activity," *Sci. Rep.*, vol. 10, no. 1, pp. 1–15, Apr. 2020, doi: 10.1038/s41598-020-63933-5.

[19] H. Cheng et al*et al.*., "Gazing point dependent eye gaze estimation," *Pattern Recognit.*, vol. 71, pp. 36–44, Nov. 2017, doi: 10.1016/j.patcog.2017.04.026.

[20] A. Duchowski, *Eye Tracking Methodology: Theory and Practice*, 2nd ed. London: Springer-Verlag, 2007.

[21] I. Hooge, K. Holmqvist, and M. Nyström, "The pupil is faster than the corneal reflection (CR): Are video based pupil-CR eye trackers suitable for studying detailed dynamics of eye movements?," *Vis. Res.*, vol. 128, pp. 6–18, Nov. 2016, doi: 10.1016/j.visres.2016.09.002.

[22] H. S. Yoon, N. R. Baek, N. Q. Truong, and K. R. Park, "Driver gaze detection based on deep residual networks using the combined single image of dual near-infrared cameras," *IEEE Access*, vol. 7, pp. 93448–93461, 2019, doi: 10.1109/ACCESS.2019.2928339.

[23] M. Horsley, M. Eliot, B. A. Knight, and R. Reilly, Eds., *Current Trends in Eye Tracking Research*. Cham: Springer International Publishing, 2014.

[24] M. J. Doughty, "Further Assessment of gender- and blink pattern-related differences in the spontaneous eyeblink activity in primary gaze in young adult humans," *Optometry Vis. Sci.*, vol. 79, no. 7, pp. 439–447, Jul. 2002.

[25] A. Maffei and A. Angrilli, "Spontaneous eye blink rate: An index of dopaminergic component of sustained attention and fatigue," *Int. J. Psychophysiol.*, vol. 123, pp. 58–63, Jan. 2018, doi: 10.1016/j.ijpsycho.2017.11.009.

[26] P. Majaranta, U. Ahola, and O. Špakov, "Fast gaze typing with an adjustable dwell time," in *Proc. ACM CHI 2009: Conf. Hum. Factors Comput. Syst.*, 2009, pp. 357–360.

[27] J. Lazar, J. H. Feng, and H. Hochheiser, "Chapter 1 - Introduction to HCI research," in *Research Methods in Human Computer Interaction* 2nd ed., J. Lazar, J. H. Feng, and H. Hochheiser, Eds. Boston: Morgan Kaufmann, 2017, pp. 1–24.

[28] P. R. Lourenço, W. W. Abbott, and A. A. Faisal, "Supervised EEG ocular artefact correction through eye-tracking," in *Proc. Adv. Neurotechnol., Electron. Inform.: Revised Sel. Papers 2nd Int. Congr. Neurotechnol., Electron. Inform. (NEUROTECHNIX 2014), October 25-26*, Rome, Italy, A. R. Londral and P. Encarnação, Eds. Cham: Springer International Publishing, 2016, pp. 99–113.

[29] S. He and Y. Li, "A single-channel EOG-based speller," *IEEE Trans. Neural Syst. Rehabil. Eng.*, vol. 25, no. 11, pp. 1978–1987, Nov. 2017, doi: 10.1109/TNSRE.2017.2716109.

[30] A. de Marcellis *et al.*, "Giant magnetoresistance (GMR) sensors for 0.35μm CMOS technology sub-mA current sensing," in *Proc. IEEE Sensors*, Nov. 2014, pp. 444–447, doi: 10.1109/ICSENS.2014.6985030.

[31] Y. Wu, L. Xiao, S. Hou, Z. Gao, and L. Han, "High Tc TMR-superconducting mixed sensor: Fabrication and performance," *IEEE Trans. Appl. Supercond.*, vol. 29, no. 1, pp. 1–5, Jan. 2019, doi: 10.1109/TASC.2018.2867790.

[32] S. Zuo, K. Nazarpour, and H. Heidari, "Device modeling of MgO-Barrier tunneling magnetoresistors for hybrid spintronic-CMOS," *IEEE Electron Device Lett.*, vol. 39, no. 11, pp. 1784–1787, Nov. 2018, doi: 10.1109/LED.2018.2870731.

[33] S. D. Muthukumaraswamy, "High-frequency brain activity and muscle artifacts in MEG/EEG: A review and recommendations," *Front. Human Neurosci.*, vol. 7, p. 136, 2013, doi: 10.3389/fnhum.2013.00138.

[34] J. M. Furman and F. L. Wuyts, "Vestibular laboratory Testing," in *Aminoff's Electrodiagnosis in Clinical Neurology*, Elsevier, 2012, pp. 699–723.

[35] N. Locatelli and V. Cros, "Basic spintronic transport phenomena," in *Introduction to Magnetic Random-Access Memory*, B. Dieny, R. B. Goldfarb, and K. Lee, Eds. Hoboken, NJ, USA: John Wiley & Sons, Inc., 2016, pp. 1–28.

[36] H. Kaiju et al*et al.*., "Robustness of voltage-induced magnetocapacitance," *Sci. Rep.*, vol. 8, no. 1, pp. 1–10, Oct. 2018, doi: 10.1038/s41598-018-33065-y.

[37] S. Bandyopadhyay and M. Cahay, *Introduction to Spintronics*. CRC Press, 2015.

[38] Y.-F. Liu, X. Yin, Y. Yang, D. Ewing, P. J. De Rego, and S.-H. Liou, "Tunneling magnetoresistance sensors with different coupled free layers," *AIP Adv.*, vol. 7, no. 5, May 2017, Art. no. 056666, doi: 10.1063/1.4977774.

[39] M. Yuan et al*et al.*., "Electronic contact lens: A platform for wireless health monitoring applications," *Adv. Intell. Syst.*, vol. 2, no. 4, 2020, Art. no. 1900190, doi: 10.1002/aisy.201900190.

[40] M. Villegas, Z. Cetinic, A. Shakeri, and T. F. Didar, "Fabricating smooth PDMS microfluidic channels from low-resolution 3D printed molds using an omniphobic lubricant-infused coating," *Analytica Chimica Acta*, vol. 1000, pp. 248–255, Feb. 2018, doi: 10.1016/j.aca.2017.11.063.

[41] R. Chalmers, "Overview of factors that affect comfort with modern soft contact lenses," *Contact Lens Anterior Eye*, vol. 37, no. 2, pp. 65–76, Apr. 2014, doi: 10.1016/j.clae.2013.08.154.

[42] M. X. Chu et al*et al.*., "Soft contact lens biosensor for in situ monitoring of tear glucose as non-invasive blood sugar assessment," *Talanta*, vol. 83, no. 3, pp. 960–965, Jan. 2011, doi: 10.1016/j.talanta.2010.10.055.

[43] M. Chu et al*et al.*., "Biomedical soft contact-lens sensor for in situ ocular biomonitoring of tear contents," *Biomed. Microdevices*, vol. 13, no. 4, pp. 603–611, Aug. 2011, doi: 10.1007/s10544-011-9530-x.

[44] C.-H. Lin, Y.-H. Yeh, W.-C. Lin, and M.-C. Yang, "Novel silicone hydrogel based on PDMS and PEGMA for contact lens application," *Colloids Surfaces B: Biointerfaces*, vol. 123, pp. 986–994, Nov. 2014, doi: 10.1016/j.colsurfb.2014.10.053.

[45] E. Paz, S. Serrano-Guisan, R. Ferreira, and P. P. Freitas, "Room temperature direct detection of low frequency magnetic fields in the 100 pT/Hz0.5 range using large arrays of magnetic tunnel junctions," *J. Appl. Phys.*, vol. 115, no. 17, Jan. 2014, Art. no. 17E501, doi: 10.1063/1.4859036.

[46] S.-J. Ahn, T. Kato, H. Kubota, Y. Ando, and T. Miyazaki, "Bias-voltage dependence of magnetoresistance in magnetic tunnel junctions grown on Al2O3 (0001) substrates," *Appl. Phys. Lett.*, vol. 86, no. 10, Mar. 2005, Art. no. 102506, doi: 10.1063/1.1870104.

[47] Z. Q. Lei, G. J. Li, W. F. Egelhoff, P. T. Lai, and P. W. T. Pong, "Review of noise sources in magnetic tunnel junction sensors," *IEEE Trans. Magn.*, vol. 47, no. 3, pp. 602–612, Mar. 2011, doi: 10.1109/TMAG.2010.2100814.

[48] E. Paz, R. Ferreira, and P. P. Freitas, "Linearisation of magnetic sensors with a weakly pinned free-layer MTJ stack using a three-step annealing process," *IEEE Trans. Magn.*, vol. 52, no. 7, pp. 1–4, Jul. 2016, doi: 10.1109/TMAG.2016.2525772.

[49] Y. Mendelson, "Biomedical Sensors," in *Introduction to Biomedical Engineering*, Elsevier, 2012, pp. 609–666.

[50] J. Puebla, J. Kim, K. Kondou, and Y. Otani, "Spintronic devices for energy-efficient data storage and energy harvesting," *Commun. Mater.*, vol. 1, no. 1, pp. 1–9, May 2020, doi: 10.1038/s43246-020-0022-5.

[51] J. Cao and P. P. Freitas, "Wheatstone bridge sensor composed of linear MgO magnetic tunnel junctions," *J. Appl. Phys.*, vol. 107, no. 9, Apr. 2010, Art. no. 09E712, doi: 10.1063/1.3360583.

[52] D. J. Cohen, "Look little, look often: The influence of gaze frequency on drawing accuracy," *Perception Psychophys.*, vol. 67, no. 6, pp. 997–1009, Aug. 2005, doi: 10.3758/BF03193626.

[53] C. Constable, "Earth's electromagnetic environment," *Surv. Geophys.*, vol. 37, no. 1, pp. 27–45, Jan. 2016, doi: 10.1007/s10712-015-9351-1.

[54] L. A. Francis and K. Poletkin, *Magnetic Sensors and Devices: Technologies and Applications*. CRC Press, 2017.

[55] M. Bahaz and R. Benzid, "Efficient algorithm for baseline wander and powerline noise removal from ECG signals based on discrete Fourier series," *Australas Phys. Eng. Sci. Med.*, vol. 41, no. 1, pp. 143–160, Mar. 2018, doi: 10.1007/s13246-018-0623-1.

[56] A. Fasano and V. Villani, "Baseline wander removal for bioelectrical signals by quadratic variation reduction," *Signal Process.*, vol. 99, pp. 48–57, Jun. 2014, doi: 10.1016/j.sigpro.2013.11.033.

[57] Y. Luo et al*et al.*., "A hierarchical method for removal of baseline drift from biomedical signals: Application in ECG analysis," *Sci. World J.*, vol. 2013, pp. 1–10, 2013, doi: 10.1155/2013/896056.

[58] G. N. Foulks, "Prolonging contact lens wear and making contact lens wear safer," *Amer. J. Ophthalmol.*, vol. 141, no. 2, pp. 369–373.e2, Feb. 2006, doi: 10.1016/j.ajo.2005.08.047.

[59] J. Kim et al*et al.*., "Wearable smart sensor systems integrated on soft contact lenses for wireless ocular diagnostics," *Nat. Commun.*, vol. 8, no. 1, Apr. 2017, Art. no. 14997, doi: 10.1038/ncomms14997.

[60] J. Park et al*et al.*., "Soft, smart contact lenses with integrations of wireless circuits, glucose sensors, and displays," *Sci. Adv.*, vol. 4, no. 1, Jan. 2018, Art. no. eaap9841.

[61] W. J. Lee, J. H. Kim, Y. U. Shin, S. Hwang, and H. W. Lim, "Differences in eye movement range based on age and gaze direction," *Eye*, vol. 33, no. 7, pp. 1145–1151, Jul. 2019, doi: 10.1038/s41433-019-0376-4.

[62] X. Liang, R. Ghannam, and H. Heidari, "Wrist-worn gesture sensing with wearable intelligence," *IEEE Sensors J.*, vol. 19, no. 3, pp. 1082–1090, Feb. 2019, doi: 10.1109/JSEN.2018.2880194.

[63] 'Tetris – Britannica Academic'. [Online]. Available: https://academic-eb-com.ezproxy.lib.gla.ac.uk/levels/collegiate/article/Tetris/438631. Accessed Apr. 14, 2020.

[64] J. R. Wolpaw, N. Birbaumer, D. J. McFarland, G. Pfurtscheller, and T. M. Vaughan, "Brain–computer interfaces for communication and control," *Clin. Neurophysiol.*, vol. 113, no. 6, pp. 767–791, Jun. 2002.

[65] B. Dal Seno, M. Matteucci, and L. T. Mainardi, "The utility metric: A novel method to assess the overall performance of discrete brain–computer interfaces," *IEEE Trans. Neural Syst. Rehabil. Eng.*, vol. 18, no. 1, pp. 20–28, Feb. 2010, doi: 10.1109/TNSRE.2009.2032642.

[66] M. M. N. Mannan, M. A. Kamran, S. Kang, H. S. Choi, and M. Y. Jeong, "A hybrid speller design using eye tracking and SSVEP brain–computer interface," *Sensors (Basel)*, vol. 20, no. 3, p. 891, Feb. 2020, doi: 10.3390/s20030891.

[67] A. Fathi and F. Abdali-Mohammadi, "Camera-based eye blinks pattern detection for intelligent mouse," *SIViP*, vol. 9, no. 8, pp. 1907–1916, Nov. 2015, doi: 10.1007/s11760-014-0680-1.

[68] H. Sato, K. Abe, S. Ohi, and M. Ohyama, "An automatic classification method for involuntary and two types of voluntary blinks," *Electron. Commun. Jpn.*, vol. 100, no. 10, pp. 48–58, 2017, doi: 10.1002/ecj.11986.

[69] F. You, Y. Li, L. Huang, K. Chen, R. Zhang, and J. Xu, "Monitoring drivers' sleepy status at night based on machine vision," *Multimedia Tools Appl.*, vol. 76, no. 13, pp. 14869–14886, Jul. 2017, doi: 10.1007/s11042-016-4103-x.

[70] H. Singh and J. Singh, "Real-time eye blink and wink detection for object selection in HCI systems," *J. Multimodal User Interfaces*, vol. 12, no. 1, pp. 55–65, Mar. 2018, doi: 10.1007/s12193-018-0261-7.

[71] P. Kowalczyk and D. Sawicki, "Blink and wink detection as a control tool in multimodal interaction," *Multimedia Tools Appl.*, vol. 78, no. 10, pp. 13749–13765, May 2019, doi: 10.1007/s11042-018-6554-8.

[72] Q. Huang *et al.*, "An EOG-based human–machine interface for wheelchair control," *IEEE Trans. Biomed. Eng.*, vol. 65, no. 9, pp. 2023–2032, Sep. 2018, doi: 10.1109/TBME.2017.2732479.

[73] P. Graybill and M. Kiani, "Eyelid drive system: An assistive technology employing inductive sensing of eyelid movement," *IEEE Trans. Biomed. Circuits Syst.*, vol. 13, no. 1, pp. 203–213, Feb. 2019, doi: 10.1109/TBCAS.2018.2882510.